



Numerical simulation of stress behavior of dowel–brick structures in TMSR

Hui-Qing Fan¹ · Chao-Chao Huang¹ · Xiao Wang¹ · D. K. L. Tsang¹ ·
Xiao-Chun Zhang¹ · Xiao-Yan Wang¹ · Shi-Feng Zhu¹

Received: 25 December 2019 / Revised: 11 March 2020 / Accepted: 11 March 2020 / Published online: 4 May 2020
© China Science Publishing & Media Ltd. (Science Press), Shanghai Institute of Applied Physics, the Chinese Academy of Sciences, Chinese Nuclear Society and Springer Nature Singapore Pte Ltd. 2020

Abstract As essential elements of the graphite reflector in thorium-based molten salt reactor, dowel–brick structures are used to withstand complex working loads in the reactor core and their failure may lead to serious damage of the graphite reactor core. It is crucial to investigate the stress behavior of dowel–brick structures for safe operation of the graphite reactor. In this study, three groups of finite element analyses and a strain test were carried out to investigate how the geometric parameters of the dowels affect the stress behavior of the dowel–brick structure. The numerical results indicate that the stress behavior of a dowel–brick structure is significantly affected by the diameter, length, and aspect ratio of the dowels. The maximum stress in the lower and upper bricks decreases with an increase in the dowel length. The location of maximum stress on both lower and upper bricks shifts from the root of the socket to the edge of that socket beside the contact region, as the length of the dowel increases. The shift of the maximum stress location occurs earlier for the upper bricks than for the lower bricks. The results of strain tests show good agreement with those of numerical analyses.

Keywords Dowel–brick structure · FEA · Stress behavior · Strain test

This work was supported by the Strategic Priority Research Program of the Chinese Academy of Sciences (No. XDA02010000).

✉ Xiao-Chun Zhang
zhangxiaochun@sinap.ac.cn

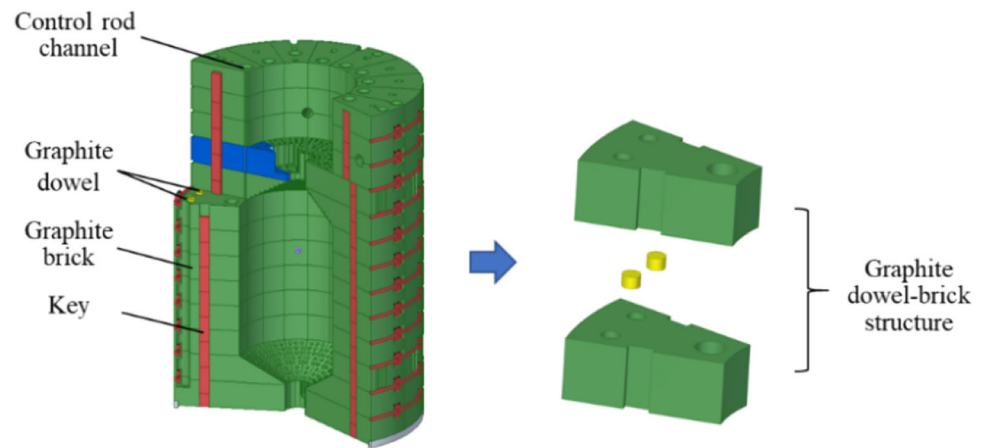
¹ Shanghai Institute of Applied Physics, Chinese Academy of Sciences, Shanghai 201800, China

1 Introduction

Graphite is an excellent moderator, and it has been widely applied in the cores of graphite reactors such as advanced gas-cooled reactor (AGR) [1], high-temperature engineering test reactor (HTTR) [2], and high-temperature reactor pebble bed module (HTR-PM) [3]. In thorium-based molten salt reactor (TMSR) [4], graphite material has also been used to form a reflector for the reactor core, as shown in Fig. 1. The graphite reflector in TMSR consists of thousands of graphite bricks, dowels, and keys. The bricks are essential and major elements of the reflector and are stacked axially to form the graphite core array. Graphite dowels and keys are designed to connect adjacent bricks and to maintain the structural integrity and dimension stability when the graphite core is subjected to complex working conditions including earthquakes, high temperature, and fast neutron irradiation. Because the dowel–socket structures and key–keyway structures are the primary components intended to withstand a variety of loads, their failures may lead to serious damage to the graphite reactor core. However, dowel–socket structures are more crucial for the graphite core in TMSR than key–keyway structures are because the gaps between the former are smaller than those between the latter. It is, therefore, necessary to investigate the dowel–brick structure in TMSR.

To ensure the structural integrity of the graphite component, a significant amount of researches have been performed on seismic tests [5]. Seismic tests on one-fifth scale models were carried out to investigate the vibration characteristics of graphite core components in HTGR [6], and the experimental data were used to verify analytical models. For HTTR, a series of tests on graphite components have also been performed. For example, the vibrational

Fig. 1 (Color online) Graphite reactor core of TMSR



characteristics of the core-bottom structure [7] and failure tests on core-support post-seat components [8] have been studied. Dynamic tests on two graphite bricks in TMSR, in which the effect of molten salt on the graphite bricks was considered, have been conducted by Zhong et al. [9]. Other similar seismic tests or analyses have been performed such as HTR-PM [10, 11], AGR [1], and medium-sized HTR [12]. It is important to conduct seismic tests to identify the dynamic characteristics of the graphite components of the whole graphite core. However, it is difficult and costly to grasp its characteristics by tests or analyses because of the complexity of the graphite core. Therefore, the graphite core in AGR was simplified in one-, two-, and three-dimensional models using the computer code AGRCOR [13]. A 2-D code SONATINA-2V [14] was developed by Japan Atomic Energy Research Institute (JAERI), in which a graphite block was treated as a rigid body with three degrees of freedom and horizontal collisions of blocks were represented by springs and viscous dampers. More recently, many simplified models for the graphite components have been developed (i.e., mass point–connector model for HTR-PM [15], rigid body–spring model for TMSR [4], and spring–damper model for AGR [16]).

Compared with seismic tests and analyses, the studies on the stress behavior of graphite components are limited. In HTTR [17], the stress behavior of the key–keyway structure was simulated using the FEA code ABAQUS. In this analysis, the structure was simplified to a 2-D model. The high-stress-concentration area of the structure was found at around 40° – 70° along the direction of the load applied. Additionally, Ishihara et al. [18] carried out both FEA and fracture tests on a dowel–socket system in HTTR. In this work, crack lines were observed along the direction about $\pm 60^{\circ}$ to the direction of the applied load. The test results were in good agreement with the high-stress regions in the analyses. For HTR-PM [19], similar fracture tests have been performed on dowel–brick structures. Cracks caused by compression were found around the contact region, and

ones caused by tension were found beside the contact region. Similar results were obtained for TMSR [20]. Moreover, the load capacity of the dowel and socket system of HTTR was studied by Takikawa et al. [21]. In those tests, the load capacity of the dowels with a diameter of 45 mm was less than that of dowels with a diameter 55 mm, and portions with fractures were found in a ligament near a socket hole.

In the past, the dynamic characteristics of dowel–brick structures have been widely investigated using seismic tests and finite element analyses (FEA). However, researches on the stress behavior of dowel–brick structures are limited; therefore, whether and how the geometric parameters of graphite dowels affect the stress behavior of the dowel–brick structure is still unknown. In this study, the stress behavior of three groups of dowel–brick structures was investigated using FEA. In addition, a strain test was carried out to verify the analysis result. It is expected that the results of this work could be used to guide improved design of the dowel–brick structures in TMSR.

2 Methodologies

2.1 FE modeling

A graphite dowel–brick structure, an essential cell of thousands of graphite components in TMSR reactor core, consists of two bricks and two dowels between the bricks, as shown in Fig. 2a. There are two sockets for the dowels on the top and bottom surfaces of each brick. For clarity, the sockets on the top surface of the upper brick and the bottom surface of the lower brick are not shown in this figure. There are two keys (not shown in Fig. 2a) and two key ways on the side surfaces of each graphite brick, and one control rod channel or other type of channel in the bricks.

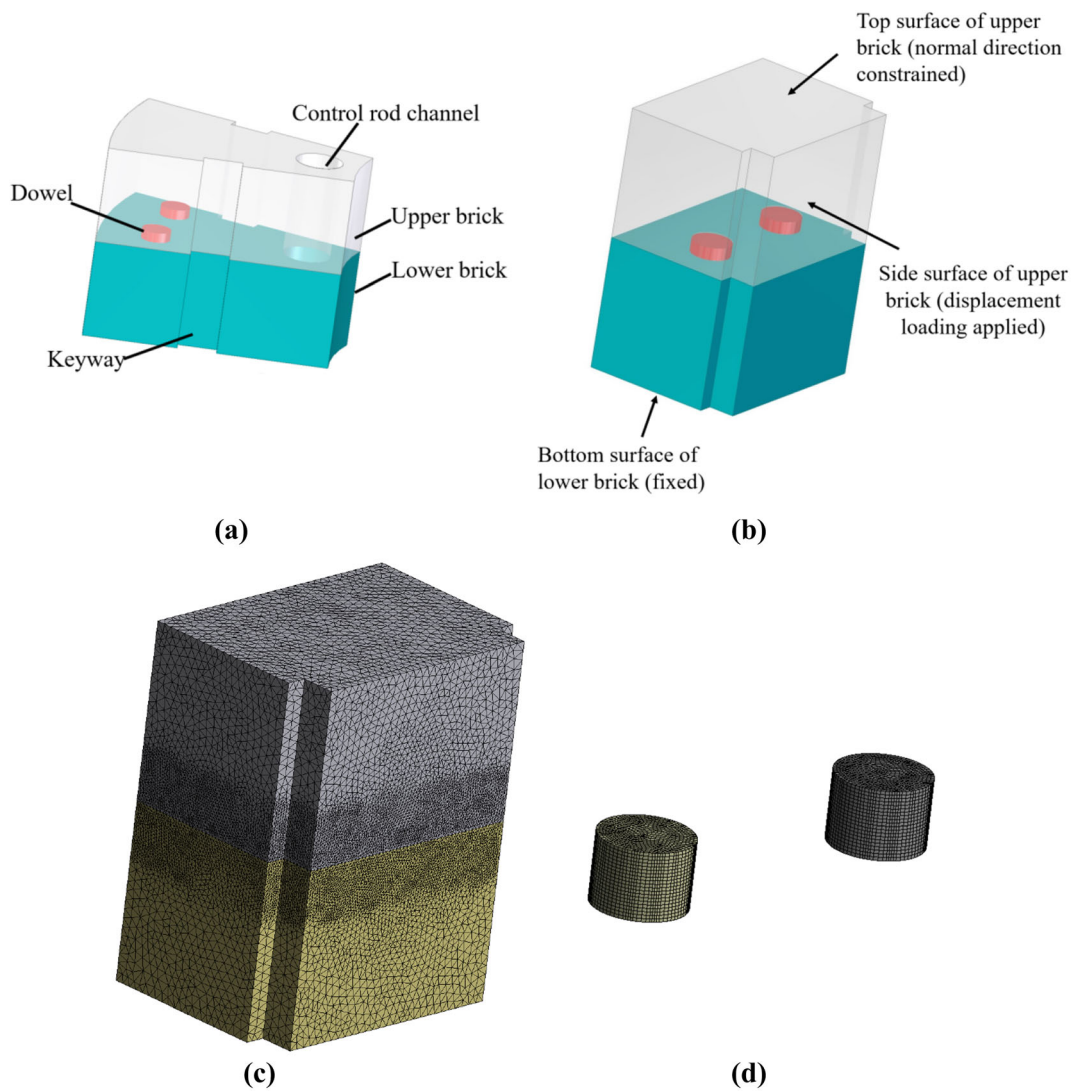


Fig. 2 (Color online) Original, simplified, and finite element model of a dowel–brick structure: **a** original model, **b** simplified model and boundary conditions, **c** FE mesh of dowel–brick structure, and **d** FE mesh of dowel

In the FEA, both graphite bricks were simplified to cuboid ones with dimensions of 490 mm × 350 mm × 300 mm, which is approximately the size of the original brick design, excluding the part containing the control rod channel. Half of the keyways were retained on both side surfaces of FEM; the same as those in the original graphite brick is shown in Fig. 2b.

To investigate the effect of the geometric parameters of the dowels on the stress behavior of the dowel–brick structure, three groups of analyses (Groups A, B, and C) were carried out, in which dowels of different lengths, diameters, and aspect ratios were considered. In each group, six kinds of dowels were involved with the same diameter, but with varied lengths (48, 58, 68, 78, 88, or 98 mm). Dowels with diameters of 69.5, 89.5, and 99.5 mm were designed for Groups A, B, and C,

respectively. For all analytical models, the clearances were kept the same: The dowels were 2 mm less in length and 0.5 mm less in diameter than the sockets. The parameters of all the dowels and sockets are listed in Table 1.

Both the dowels and bricks in the TMSR were made of NG-CT-10 graphite fabricated by Chengdu Carbon Co., Ltd., which was also used in the FEA. The typical material parameters of NG-CT-10 graphite are listed in Table 2.

The boundary conditions in the FEA were simplified from those that exist in the graphite reactor core in TMSR. The bottom surface of the lower brick was fixed. The normal direction of the top surface of the upper brick was constrained to prevent overturn of the upper brick. To simulate the shear load applied to the dowel–brick structure, a cyclic horizontal displacement of 0.85 mm was applied to the side surface of the upper brick in the

Table 1 Geometric parameters of the dowels and sockets

Group	Model	Diameter (mm)	Length (mm)
A	1	69.5/70	48/50
	2		58/60
	3		68/70
	4		78/80
	5		88/90
	6		98/100
B	7	89.5/90	48/50
	8		58/60
	9		68/70
	10		78/80
	11		88/90
	12		98/100
C	13	99.5/100	48/50
	14		58/60
	15		68/70
	16		78/80
	17		88/90
	18		98/100

Table 2 Typical material parameters of NG-CT-10 graphite

Property	Values
Grain size (μm)	25
Bulk density (kg/m^3)	1.88×10^3
Flexural strength (MPa)	31.4
Tensile strength (MPa)	23.2
Compressive strength (MPa)	78.0
Young's modulus (GPa)	9.0
Poisson's ratio	0.2

direction perpendicular to the position of the dowels, as presented in Fig. 2b.

In all cases, ANSYS solid 186 elements were used for the graphite dowel and solid 187 elements were used for the graphite brick meshing shown in Fig. 2c and d. The solid 186 and 187 elements are 3-D quadratic hexahedron and tetrahedron elements (respectively). A mesh sensitivity study was done to make sure that the analysis results were mesh independent. In numerical analyses, all contacts between the upper and lower bricks, and between bricks and dowels, were defined as frictional contacts with a friction coefficient of 0.2.

For all models, the same loads and boundary conditions were applied. All the numerical analyses of the dowel–

brick structures were performed by the general-purpose FE software ANSYS.

2.2 Experimental method

One specimen made of the NG-CT-10 graphite was fabricated for the strain tests on the dowel–brick structure in TMSR. The geometric parameters of the specimen were the same as those of Model 8 in the FEA. The strain tests were performed using the test setup shown in Fig. 3a, in which the lower brick was mounted on the test bench and fixed using precast dies and two parallel jacks. The horizontal force was applied to one side of the upper brick using a loading device in the same direction as used in the FEA. To prevent overturn of the upper brick, a constant perpendicular force was imposed on the top surface of the upper brick by a vertical jack. The force applied on the top and side surfaces of the upper brick and the displacement of the upper brick were all monitored throughout the test.

The horizontal load was a cyclic force that consisted of the two stages shown in Fig. 3b. In the first stage, the loading force was 50 kN and the same load was applied twice. The load in the second stage was as the same as that in the first one, except that the force applied was 100 kN. The first stage of loading was applied as preloading, while the second was used for the actual strain test.

Because the peak value of the maximum principal stress of the dowel–brick structure appeared around the sockets, strain gauges were fixed evenly on the edges of two sockets (Fig. 3c). In the test, 16 strain rosettes (shown in Fig. 3d) were used to determine the strain state around the socket.

3 Results and discussion

3.1 Analysis results

Figure 4a–c presents the stress state of the dowel–brick structure named Model 1 in Group A under displacement loading of 0.85 mm. Considering that graphite is a brittle material and that the dowels in the dowel–brick structure are subjected to shear load, maximum principal stress for the upper and lower bricks and shear stress for the graphite dowel are shown. The peak maximum principal stress of the dowel–brick structure is 20.2 MPa, which occurs on the root of the dowel socket in the lower brick. The higher stress regions in the lower brick, in which the stress decreases gradually from 20.2 to 12.9 MPa, occur from the root of the socket to its edge on both sides of the contact region, between the dowel and socket. The two higher stress regions in the same socket are generally symmetrical (shown in Fig. 4a). For convenience, these higher stress regions are called ligaments for short and the contact

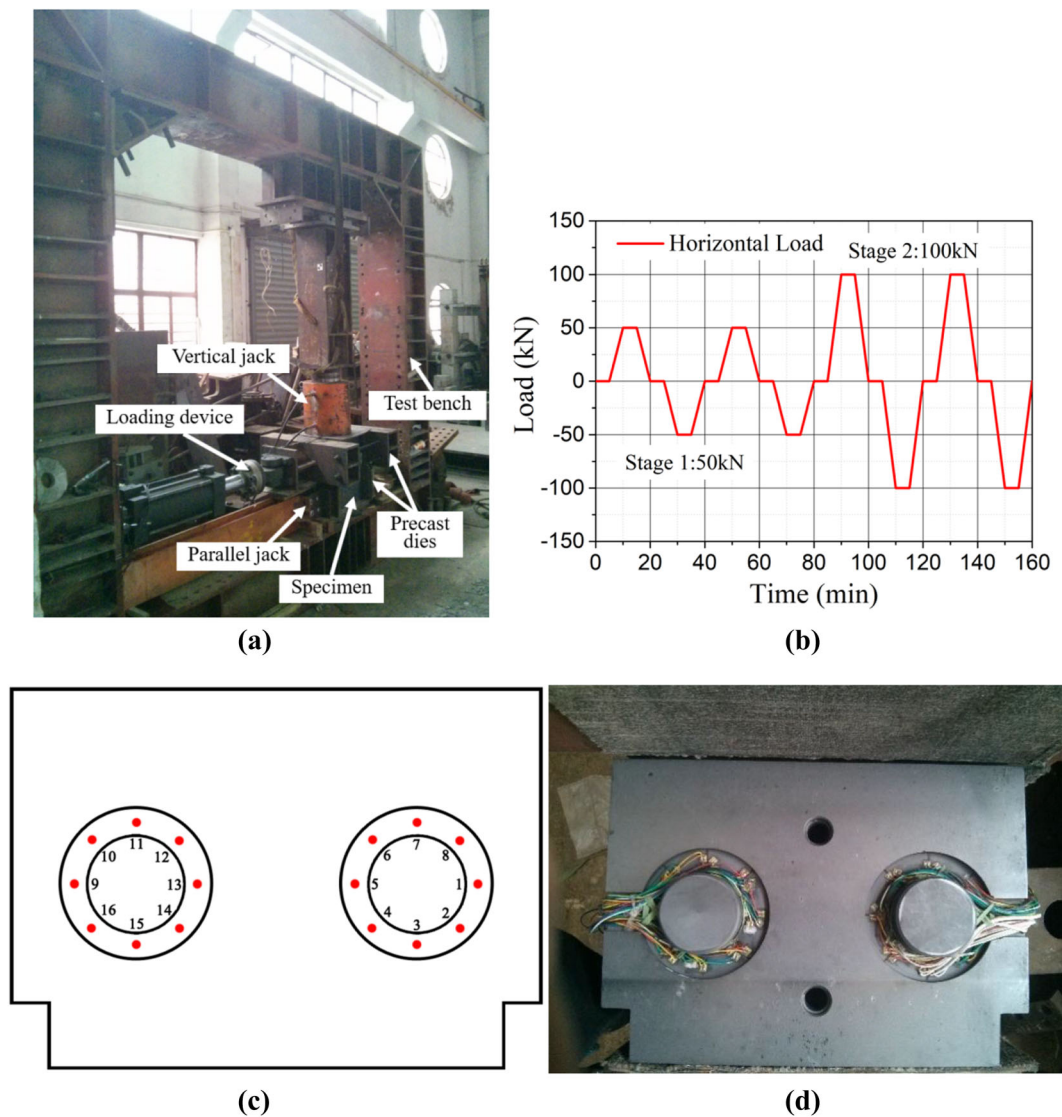


Fig. 3 (Color online) Strain test setup: **a** test setup, **b** cyclic horizontal load, **c** schematic layout of the strain gauges, and **d** actual layout of the strain gauges

region between dowel and socket is abbreviated as the “contact region” in this paper. The stress level of the regions around the ligaments is higher than that in other parts, in all of which the stress is less than 1 MPa. The stress state of the upper brick is analogous to that of the lower brick, which is shown in Fig. 4b. The maximum stress of the upper brick is also located on the socket root, which is 13.1 MPa smaller than that of the lower brick. The maximum shear stress of the graphite dowel was 6.5 MPa in the contact region.

The analytic results for Model 4 in Group A are shown in Fig. 4d and e. It can be observed from the figure that the maximum stress of Model 4 (14.5 MPa) is located in the lower brick. The stress state of the lower brick of Model 4 is similar to that of Model 1, except that the location of the

maximum stress appears on the edge of a socket beside the contact region. Almost the same stress state for the lower bricks was obtained in Model 5 and 6 in Group A. Similar phenomena occurred in the upper bricks of Models 2–6 in Group A.

Figure 4 shows two representative stress states; the others are similar to them, but are not shown in this paper. All of FEA results are shown in Table 3. It can clearly be seen that the locations of maximum stress for both lower and upper bricks shifted from the root of the sockets to their edges as above-mentioned, not only in Group A, but also in Groups B and C. Nevertheless, the transfer points of the lower bricks appear at dowel lengths of 78, 98, and 98 mm for Groups A, B, and C, respectively. For the upper bricks, the transfer points were found at dowel lengths of

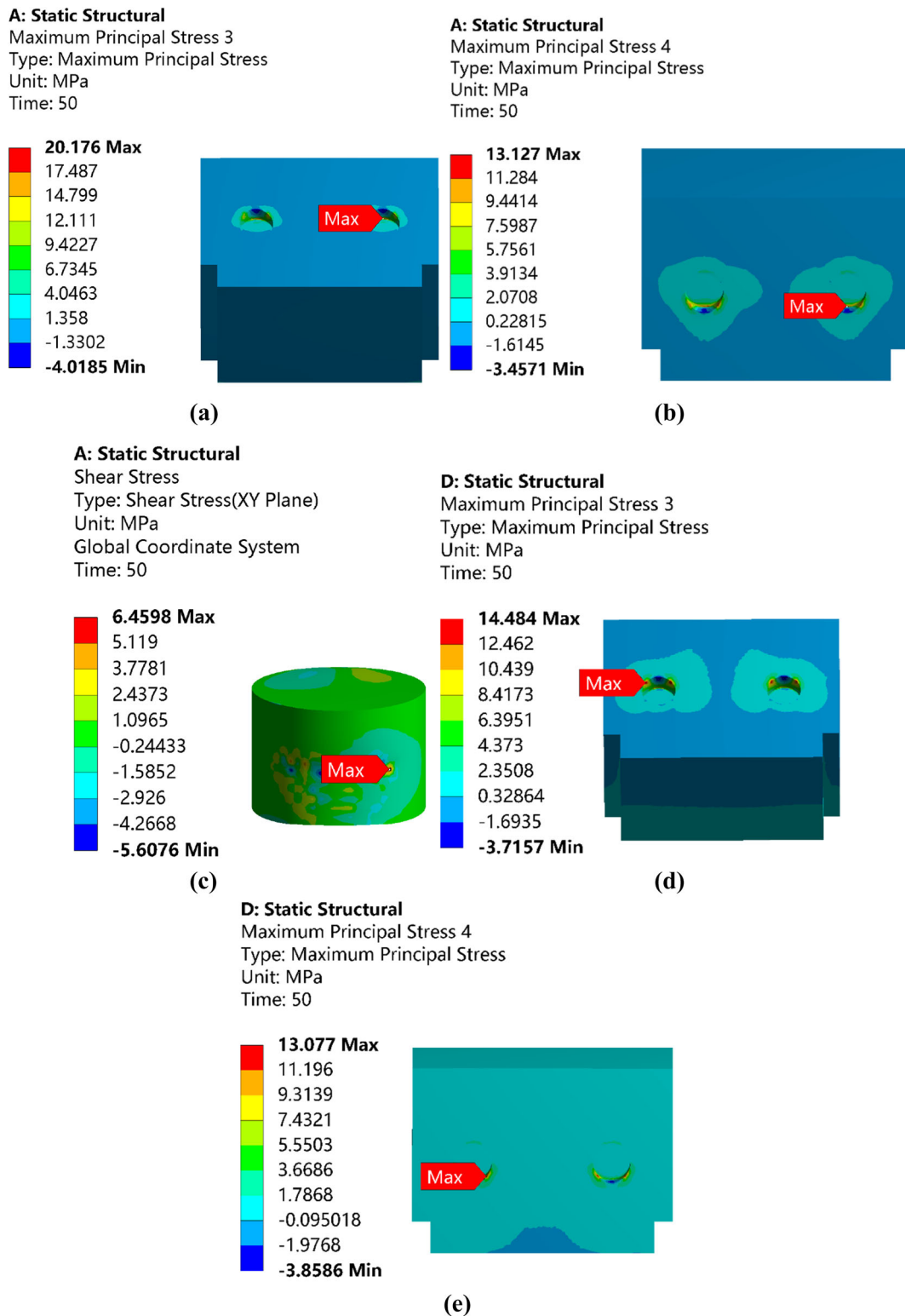


Fig. 4 (Color online) Stress state of the dowel–brick structure named Model 1 of Group A: **a** lower brick of Model 1, **b** upper brick of Model 1, **c** dowel of Model 1, **d** lower brick of Model 4, and **e** upper brick of Model 4

58, 78, and 78 mm for Groups A, B, and C, respectively. Moreover, the above transfers occurred with a dowel aspect ratio of 1.1 for the lower bricks and 0.8 for the upper brick

in the models of Group A, while for Groups B and C, such transfer points occurred for dowels with an aspect ratio of 1.1 and 1.0 for lower brick and 0.9 and 0.8 for upper bricks.

Table 3 Results of the finite element analyses

Group	Model	Dowel and socket			Location of the maximum stress	
		Diameter (mm)	Length (mm)	Aspect ratio of dowel	Lower brick	Upper brick
A	1	69.5/70	48/50	0.69	Root of the socket	Root of the socket
	2		58/60	0.83		Edge of socket beside the contact region
	3		68/70	0.98	–	
	4		78/80	1.12	Edge of socket beside the contact region	
	5		88/90	1.27		
	6		98/100	1.41		
B	7	89.5/90	48/50	0.54		Root of the socket
8	58/60		0.65			
9	68/70		0.76			
10	78/80		0.87		Edge of socket beside the contact region	
11	88/90		0.98			
12	98/100		1.09	Edge of socket beside the contact region		
C	13	99.5/100	48/50	0.48	Root of the socket	Root of the socket
	14		58/60	0.58		
	15		68/70	0.68		
	16		78/80	0.78		Edge of socket beside the contact region
	17		88/90	0.88		
	18		98/100	0.98	Edge of socket beside the contact region	

It is noteworthy that numerical convergence was difficult in the case of Model 3 in Group A, in which the dowel had an aspect ratio of “1”. Similar phenomena occurred in three additional numerical computations in which the models had dowels with a diameter of 49.5, 59.5, and 79.5 mm, but all with an aspect ratio of “1”. However, this situation would be changed if the diameter of a graphite dowel was big enough (e.g., 89.5 mm in Model 11 and 99.5 mm in Model 18). It may be concluded that it is difficult to form a state of stable contact between a dowel and its socket under displacement loading when the graphite dowel is one with smaller diameter and aspect ratio of “1”. This situation should be avoided in the design of dowels.

The maximum principal stress on the edge of the Socket A in the lower brick of Model 4 is presented in Fig. 5, in which the contact region is defined as 0°. The stress on the edge of the socket is symmetrically distributed around the contact region. The contact region is most influenced by compression, while both peak positions are most influenced by tension. The two high-stress-concentration areas are observed along the directions of – 45° and 51° relative to the applied load, in which the two peak values (14.0 and

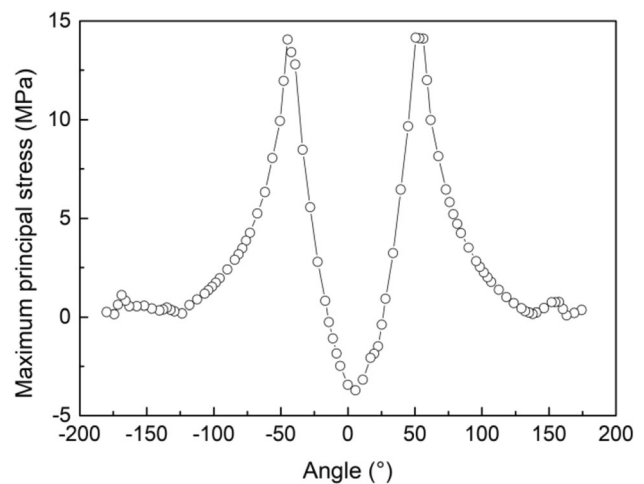


Fig. 5 Maximum principal stress on the edge of the Socket A in the lower brick of Model 4

14.2 MPa) can be found. Away from the peak positions, the stress decreases significantly.

With an increase in the dowel length, the maximum stress (25.2 MPa) in the lower brick in Group B ($\phi 89.5$) decreases significantly to 15.0 MPa and then gradually, even more to 12.4 MPa. Finally, it reaches an approximate

constant value (12.4 MPa), as shown in Fig. 6a. In Groups A ($\phi 69.5$) and C ($\phi 99.5$), the same trends of stress change happen. In addition, the above two turning points of stress are found at aspect ratios of about 0.8 and 1.0–1.1 for the three groups, as shown in Fig. 6b. No apparent relationship between the maximum stress of the lower brick and the

diameter of the dowels is observable in Fig. 6a. Nevertheless, it is noteworthy that the maximum stress of the lower brick decreases as the dowel diameter increases when the aspect ratios of the dowels are equal, as shown in Fig. 6b. However, when the aspect ratio of a dowel is between 0.5 and 0.8, for lower bricks with dowel diameter

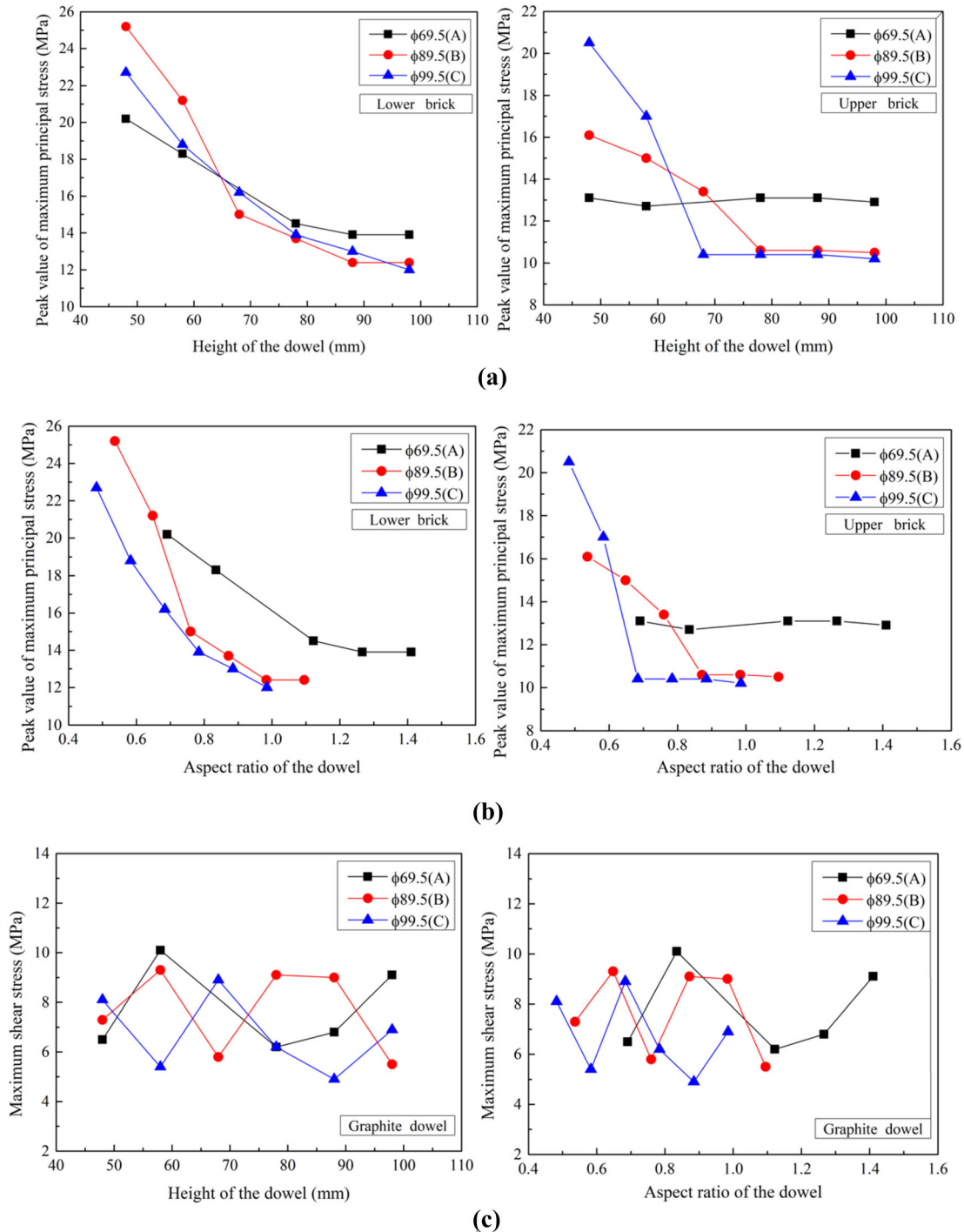


Fig. 6 (Color online) Relationship of maximum stress vs the geometric parameter of the dowels: **a** peak value of the maximum principle stress of a graphite brick vs dowel length, **b** peak value of

the maximum principle stress of a graphite brick vs dowel aspect ratio (length to diameter), and **c** maximum shear stress of a dowel vs dowel length and aspect ratio (length to diameter)

larger than $\phi 89.5$, the stress significantly decreases with an increase in the diameter. When the aspect ratio of a dowel is between 0.8 and 1.1, for lower bricks with dowel diameter less than $\phi 89.5$, the stress significantly decreases with increased diameter. It is worth noting that all the above-mentioned conclusions for lower bricks are appropriate for dowel–brick structures because the maximum stress of dowel–brick structures is located in the lower bricks.

It is shown in Fig. 6a that the relationship between the maximum stress of an upper brick and the dowel length is not consistent with that of a lower brick. For Group A ($\phi 69.5$), the maximum stress on an upper brick stays approximately stable, with some trivial fluctuations with an increase in the dowel length. Nevertheless, the maximum stress decreases slightly for Group B ($\phi 89.5$) and significantly for Group C ($\phi 99.5$) with an increase in the dowel length (< 68 mm). However, as the dowel length increases above 68 mm, the maximum stress just fluctuates slightly with an increase in the dowel length. Moreover, when the dowel length is less than 58 mm, the larger the diameter of the dowel is, the higher the maximum stress level of an upper brick will be. In contrast, when the dowel diameter is higher than 78 mm, the larger the diameter of the dowel is, the lower the maximum stress level of an upper brick will be. For the dowel length between 58 and 78 mm, an obvious transition region can be observed. The relationship between maximum stress of an upper brick and the aspect ratio of a dowel is similar to that between the stress and dowel length shown in Fig. 6b. Furthermore, when the aspect ratio of the dowel is low, the maximum stress level increases with an increase in the dowel diameter. However, when the aspect ratio is high enough, the stress level decreases as the diameter of the dowel increases. A transition region is found when the aspect ratio is between 0.6 and 0.8.

The relationship of maximum shear stress of the dowel and its parameters is shown in Fig. 6c. For all dowels in the three groups, the maximum shear stresses fluctuate between 5 and 10 MPa as their lengths and aspect ratios increase.

3.2 Experimental results

Figure 7 shows the maximum principal strain on the edges along two sockets in the test specimen under the force loading of 100 kN in the strain test. The maximum principal strain at each measuring point in the figure is calculated according to three values given by the right-angle strain. It can be seen from Fig. 7a that two high-stress-concentration regions appear symmetrically around Socket A, along the directions -45° and 45° relative to the force loading direction. The maximum strain occurs in the

region in the direction at -45° . The strain of the region in the direction of 45° is a little smaller than that of -45° . For Socket B, the two high-stress-concentration regions are also observed along the directions at -45° and 45° , and the maximum strain is in the direction at 45° .

3.3 Comparison of numerical and experimental results

Because of displacement and force loading applied in the FEA and strain test, respectively, numerical and experimental results cannot be compared directly except the high-stress-concentration region (shown in Fig. 7). Under external load, the two high-stress regions around Socket A in the FEA are in good agreement with those in the strain test. The maximum strains in the two regions are almost the same, and the situation of Socket B is the same as that of Socket A.

3.4 Discussion

For a lower brick, the maximum stress decreases with an increase in the dowel length (with the same diameter) and diameter (with the same aspect ratio). This is because the increase in dowel length or diameter will cause an increase in the contact region. However, when the dowel length is less than 58 mm, it is still unknown why the variation tendency of the maximum stress of an upper brick is opposite to that of a lower brick. More numerical analyses or more detailed tests should be able to explain this difference.

The NG-CT-10 graphite is a brittle material, and its tensile strength is less than one-third of its compressive strength based on the data listed in Table 2. Under external load, both upper and lower bricks are subjected to significant tensile stress, except in the contact region. The tensile stress is a primary factor leading to the initiation of cracks in the graphite bricks. This has been demonstrated by Shi [19] using strain tests and static tests on dowel–brick structures in HTR-PM. In addition, the stress level of a lower brick is higher than that of an upper brick. Consequently, the lower bricks will be the weakest ones in dowel–brick structures. Earlier test results [20] showed that 90% of the lower bricks of dowel–brick structures in TMSR failed under the same load. However, the failure rate of upper bricks and graphite dowels was just 40% and 30%, respectively. The analysis results in this study are consistent with the above results [20].

Previous fracture test results [19] reported that cracks were found in positions 25 and 39 beside the contact point between dowels and sockets. These two positions [19] correspond to the two regions in which high stress areas were found around sockets in this work. Therefore, the

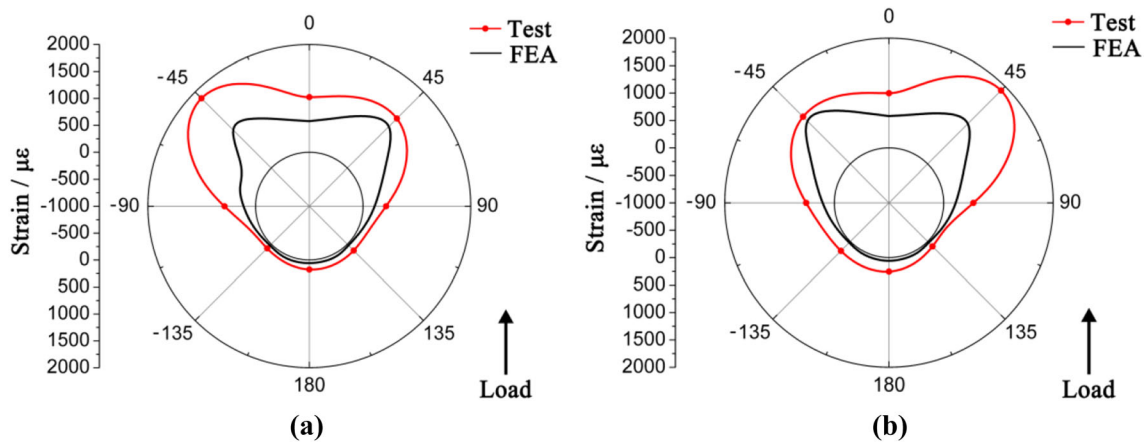


Fig. 7 Comparison of the maximum principal strain results for the strain test and FEA of **a** Socket A and **b** Socket B

high-stress-concentration regions may be the places where cracks appear in a dowel–brick structure in TMSR. This conclusion agrees well with the test results of dowel–brick structures in TMSR [20].

Based on the maximum principal stress failure theory, the location of the peak value of maximum principal stress may be the origin of crack initiation. The phenomenon that the location of maximum stress shifts from the root of a socket to its edge with an increase in dowel length may be the reason why the load capacity of a dowel–brick structure with high dowels (of the same diameter) was less than that with lower dowels in previous work in TMSR [20]. More numerical analyses and detailed tests are needed to study the failure mode of dowel–brick structures. In the failure tests on dowel and socket systems of HTTR in [21], the load capacity of a dowel with diameter 45 mm was less than that of a dowel with diameter of 55 mm. In this work, Models 4, 10, and 16, with uniform dowel length (78 mm) but different diameters (69.5, 89.5, and 99.5 mm), the maximum stress of Model 4 occurred on the edge of the socket in a lower brick and those of the latter two models appeared on the root of the socket hole. The same results were found for Models 5, 11, and 17. It seems that a graphite brick in which the maximum stress is located on the edge of a socket is more brittle than the one located on the root of the socket. This may be the reason why the load capacity of dowel–brick structure with longer (or thinner) dowels is less than that with shorter (or fatter) dowels. For the former, the cracks may initiate on the edge of the socket where the maximum stress occurs.

4 Conclusion

To investigate the effect of the geometric parameters of dowels on the stress behavior of a dowel–brick structure in TMSR, three groups of numerical analyses and one strain

test were performed. The stress behavior and strain data for the dowel–brick structures were obtained and analyzed. It can be concluded from the results that:

1. The maximum stress of a dowel–brick structure appears in the lower bricks.
2. The maximum stress in the lower and upper bricks decreases with an increase in the length of the dowels.
3. Assuming the same aspect ratio of all dowels, the maximum stress of a lower brick decreases with an increase in the dowel diameter. For the upper bricks, when the aspect ratio of the dowel is low, the maximum stress increases with an increase in the dowel diameter. However, if the aspect ratio is high enough, the maximum stress decreases with an increase in the dowel diameter. A transition region occurs when the aspect ratio of the dowels is between 0.6 and 0.8.
4. The location of maximum stress of both lower and upper bricks shifts from the root of sockets to their edges beside the contact region with an increase in the dowel length. For two bricks, the larger the diameter of the dowel, the longer the length of the dowel corresponding to the transferred point of maximum stress. The transfer of that point for an upper brick occurs earlier than for a lower brick.
5. The numerical results are in good agreement with those from the strain test.

References

1. C.R. Smith., The assessment of the Integrity of AGR core during an earthquake, IAEA Specialists' meeting on Graphite Component Structural Design (JAERI, Tokai, Japan, Sep 8–11, 1986)
2. T. Iyoku, M. Futakawa, M. Ishihara, Evaluation of aseismic integrity in the HTTR core-bottom structure. I Aseismic test for

- core-bottom structure. *Nucl. Eng. Des.* **148**, 71–81 (1994). [https://doi.org/10.1016/0029-5493\(94\)90242-9](https://doi.org/10.1016/0029-5493(94)90242-9)
3. L.B. Sun, L. Shi, H.T. Wang et al., Seismic Test and Analyses on Double-Layer Model of HTR-PM Graphite Structure, *Proceedings of the 2012 20th International Conference on Nuclear Engineering* (Anaheim, California, USA. July 30–August 3. 2012)
 4. M.Y. Cai, L. Zhu, C.C. Huang et al., A preliminary study on seismic behavior of the graphite reflector in molten salt reactor. *Nucl. Eng. Des.* **330**, 282–288 (2018). <https://doi.org/10.1016/j.nucengdes.2018.02.010>
 5. S.G. Lai, L.B. Sun, Z.M. Zhang, Seismic research on graphite reactor core. *Nucl. Tech.* **36**(4), 040604 (2013) (in Chinese)
 6. B.E. Olsen, A.J. Neylan, W. Gorcholt, Seismic test on a one-fifth scale HTGR core model. *Nucl. Eng. Des.* **36**, 355–365 (1976). [https://doi.org/10.1016/0029-5493\(76\)90028-5](https://doi.org/10.1016/0029-5493(76)90028-5)
 7. T. Iyoku, Y. Inagaki, S. Shiozawa et al., Seismic response of the high-temperature engineering test reactor core bottom structure. *Nucl. Technol.* **99**(2), 169–176 (1992). <https://doi.org/10.13182/NT92-A34687>
 8. M. Ishihara, T. Iyoku, M. Futakawa, Evaluation of aseismic integrity in the HTTR core-bottom structure III Structural integrity of core support post component. *Nucl. Eng. Des.* **148**, 91–100 (1994). [https://doi.org/10.1016/0029-5493\(94\)90244-5](https://doi.org/10.1016/0029-5493(94)90244-5)
 9. Y. Zhong, X. Yang, D. Ding et al., Dynamic characteristics identification of two graphite bricks in molten salt reactor considering fluid-structure interaction. *Nucl. Eng. Des.* **335**, 409–416 (2018). <https://doi.org/10.1016/j.nucengdes.2018.06.015>
 10. S.G. Lai, L.B. Sun, L. Shi et al., Seismic test on double-layer model of HTR-PM graphite structure. in *Proceeding of the 2014 22nd International Conference on Nuclear Engineering* (Prague, Czech Republic 7–11 July. 2014)
 11. S.G. Lai, L.B. Sun, L. Shi et al., Seismic test and analysis on HTR-PM side-reflector structure similarity model. *Atom. Energy Sci. Technol.* **50**(4), 691–697 (2016). <https://doi.org/10.7538/yzk.2016.50.04.0691> (in Chinese)
 12. W. Theymann, F. Kemter, G. Schmidt, Seismic behavior of the core structure in a medium-sized HTR, Smirt 10 (Anaheim, CA, USA 14–18 August. 1989)
 13. K. Ahmed, S. Stojko, The nonlinear seismic response of AGR core graphite brick slices-correlation of experimental and analytical results. *Earthq. Eng. Struct. D* **15**, 159–188 (1987). <https://doi.org/10.1002/eqe.4290150203>
 14. T. Iyoku, J. Smita, M. Ishihara et al., R&D on core seismic design. *Nucl. Eng. Des.* **233**, 225–234 (2004). <https://doi.org/10.1016/j.nucengdes.2004.08.011>
 15. S.G. Lai, L. Shi, X.X. Wang et al., Numerical analysis for HTR-PM graphite core structure dynamic response under seismic load. *Atom. Energy Sci. Technol.* **50**(11), 2041–2047 (2016). <https://doi.org/10.7538/yzk.2016.50.11.2041> (in Chinese)
 16. B. Kraij, S. J. Humphreys, B. G. J. Duncan, Seismic modelling of an AGR nuclear reactor core. in *Conference on Ageing Management of Graphite Reactor Cores* (Univ Cardiff, Cardiff, WALES 28–30 Nov. 2005)
 17. M. Futakawa, S. Takada, H. Takeishi et al., Evaluation of aseismic integrity in the HTTR core-bottom structure V. On the static and dynamic behavior of graphitic HTTR key-keyway structures. *Nucl. Eng. Des.* **166**, 47–54 (1996). [https://doi.org/10.1016/0029-5493\(96\)01242-3](https://doi.org/10.1016/0029-5493(96)01242-3)
 18. M. Ishihara, T. Iyoku, M. Futakawa, Evaluation of aseismic integrity in the HTTR core-bottom structure IV. Structural integrity of connecting elements between graphite components. *Nucl. Eng. Des.* **154**, 83–95 (1995). [https://doi.org/10.1016/0029-5493\(94\)00902-B](https://doi.org/10.1016/0029-5493(94)00902-B)
 19. L. Shi, L.B. Sun, Z.G. Wang et al., Graphite component testing on the load capacity of the dowel-brick structure in HTR-PM. in *Proceedings of the 2012 20th International Conference on Nuclear Engineering* (Anaheim, California, USA. July 30–August 3. 2012)
 20. H.Q. Fan, C.C. Huang, X.C. Zhang et al., Computational- and experimental-based analysis of the load capacity of dowel-brick structure of graphite component in TMSR. *Nucl. Eng. Des.* **355**, 110346 (2019). <https://doi.org/10.1016/j.nucengdes.2019.110346>
 21. N. Takikawa, M. Ishihara, T. Iyoku, S. Shiozawa., Assessment of the load capacity of the dowel and socket system in the HTTR hexagonal block. *IAEA Specialists' Meeting on Status of Graphite Development for Gas Cooled Reactors* (Tokai-Mura, Japan. 1991)